

1 **3D modelling and capacity estimation of potential targets for CO₂ storage in the Adriatic Sea,**
2 **Italy**

3 **Giampaolo Proietti^{1, x}, Marko Cvetković², Bruno Saftić², Alessia Conti¹ & Sabina Bigi¹**

4 ¹*La Sapienza University, Department of Earth Sciences, Piazzale Aldo Moro, 5, 00185 Rome, Italy*

5 ²*University of Zagreb, Faculty of Mining, Geology and Petroleum Engineering, Pierottijeva ul. 6,*
6 *10000, Zagreb, Croatia*

7 *Published in 'Petroleum Geoscience' <http://dx.doi.org/10.1144/petgeo2020-117>*

8
9 **Abstract**

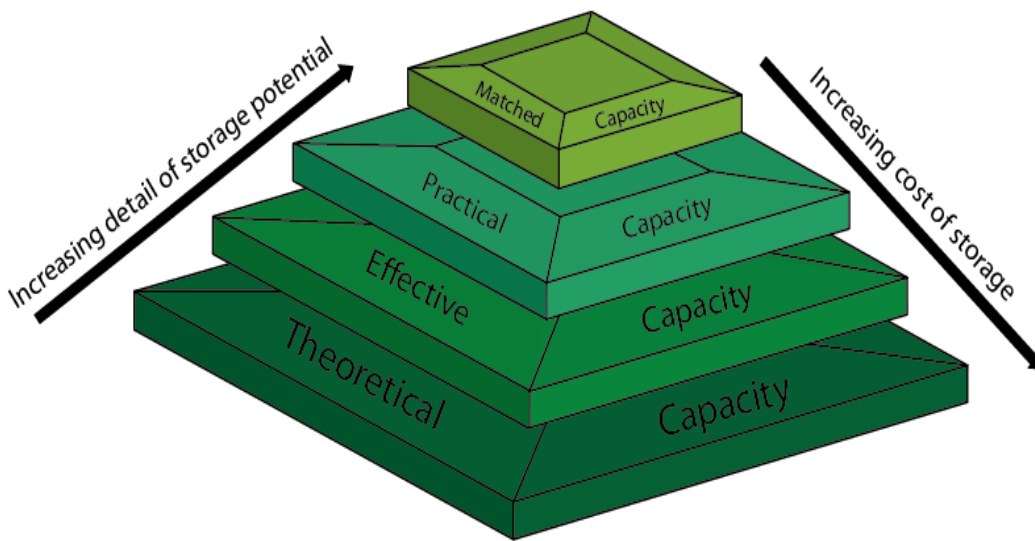
10 One of the most innovative and effective technologies developed in recent decades for reducing
11 carbon dioxide emissions to the atmosphere is CCS (Carbon Capture & Storage). It consists of
12 capture, transport and injection of CO₂ produced by energy production plants or other industries. The
13 injection takes place in deep geological formations with the suitable geometrical and petrophysical
14 characteristics to permanently trap CO₂ in the subsurface, which is called geological storage. In the
15 development process of a potential geological storage site, correct capacity estimation of the
16 injectable volumes of CO₂ is one of the most important aspects. There are various approaches to
17 estimate CO₂ storage capacities for potential traps, including geometrical equations, dynamic
18 modelling, numerical modelling, and 3D modelling. In this work, generation of three-dimensional
19 petrophysical models and equations for calculation of the storage volumes are used to estimate the
20 effective storage capacity of four potential saline aquifers in the Adriatic Sea offshore. The results
21 show how different saline aquifers, with different lithologies at favourable depths, can host a fair
22 amount of CO₂, that will imply a further and more detailed feasibility studies for each of these
23 structures. A detailed analysis is carried out for each saline aquifer identified, varying the parameters
24 of each structure identified, and adapting them for a realistic estimate of potential geological storage
25 capacity.

26
27 Of all the actions that are being developed to reduce CO₂ emissions and that can lead to a low-carbon
28 energy system, CCS (Carbon Capture and Storage) is perhaps the one that can make the greatest
29 contribution and more rapidly than other technologies. This process, which has seen significant
30 development in the last twenty years, consists of capture of CO₂ generated by power plants or other
31 large stationary industrial sources, transport through pipelines or by ships, and injection into deep
32 geological formations that have suitable characteristics to trap CO₂ (IEA, 2004; IPCC, 2005). To
33 achieve this, the potential storage sites must be identified, defining the exploitable part, and estimating
34 the volume of CO₂ that can be injected. There are many institutions and projects aiming to

35 characterize sites and estimate CO₂ storage potential in Europe, such as EU-projects EU-
36 GeoCapacity, CO₂Stop, and, in the case of Italy different research institutes and private companies
37 (<http://www.geocapacity.eu>; among many others, Vangkilde-Pedersen et al., 2009a; 2009b; Donda
38 et al., 2011; Civile et al., 2013; Volpi et al., 2015; Berenblyum et al., 2018).

39 The CO₂ storage capacity is estimated at four different levels of detail structured in a pyramid (Fig.1),
40 where from the base to the top the storage capacity value decreases as the estimate of the volume is
41 refined (Doughty et al., 2001; Bachu et al., 2007; Bradshaw et al., 2007; Kopp et al., 2009). The four
42 levels are characterized as: *theoretical* physical limit that the system can host, then the total or partial
43 volume of the pores, based on the presence of fluids; *effective*, which counts the geological and
44 engineering limitations and estimates the actual volume that can effectively be exploited; *practical*,
45 estimated considering the legal, regulatory, and economic aspects, and the presence of infrastructure;
46 and *matched*, a volume that takes into account the logistical aspects between sources and CO₂ storage
47 sites, with respect to capacity, injectivity and quantity of produced CO₂.

48



49

50

51 **Fig. 1.** Pyramid of the capacity estimation. The detail increase toward the top of the pyramid and the cost of storage
52 increases toward the bottom (After 'Bachu et al. 2007').

53

54 In this paper, we estimate the effective storage capacity of four potential structural traps for the
55 geological carbon dioxide storage in the Adriatic Sea (Italy). These are saline aquifers hosted into
56 thrust-related anticline structures buried in the Adriatic Sea under Plio-Pleistocene post-thrusting
57 deposits, named from the wells name drilled for hydrocarbons research in 80's years: Cornelia,
58 Patrizia, Elga and Serena anticlines (Fig.2). The calculations were carried out based on three-
59 dimensional models developed using Petrel software (Schlumberger, academic licence) populating

60 them with petrophysical parameters such as porosity and permeability distribution defined on the
61 basis of the available well log data. Moreover, the total pore volume obtained with this approach is
62 used to calculate the *theoretical storage* capacity using the equation proposed in the literature. Finally,
63 the introduction of an efficiency factor based on several observations also enabled estimation of the
64 effective capacity.

65

66 **Study area**

67 The Adriatic domain is the outer and younger sector of the Apennine accretionary system (Fig. 2).
68 The Adriatic Sea geology comprises the foredeep-foreland domain of the Apennine Chain (Fig. 2),
69 which is the result of convergence between the Eurasian and African plates (Boccaletti et al., 1990;
70 Bernoulli, 2001; Rosenbaum and Lister, 2004). The westward subduction of the Adria plate generates
71 the flexure of the Adria lithosphere and the eastward migration of the Apennine a fold-and-thrust belt
72 (Malinverno and Ryan, 1986; Doglioni et al., 1999).

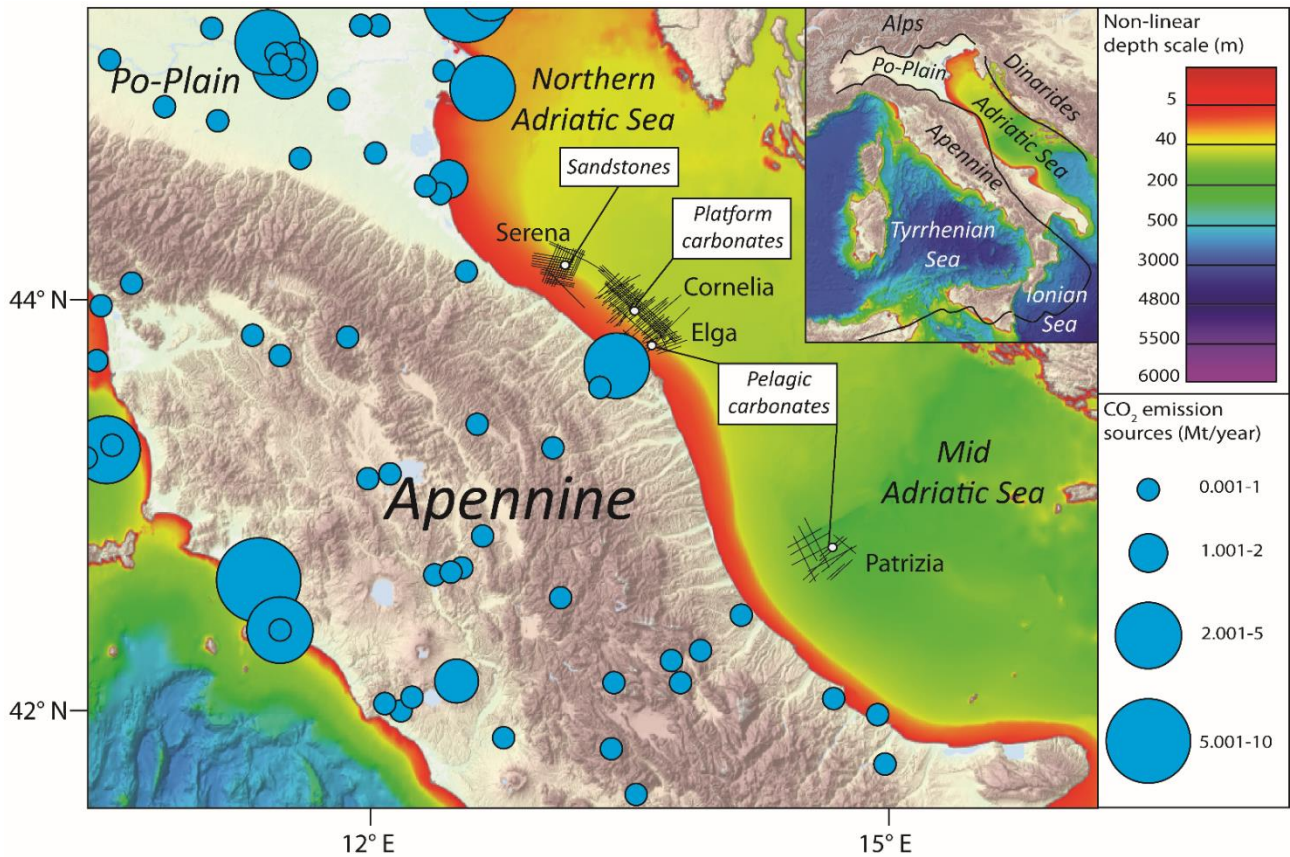
73 The Mesozoic and the Paleogene are characterized by a predominantly carbonate epi-continental
74 sedimentation linked to a complex paleogeographic configuration formed by deep basins and open
75 platforms (Calamita and Deiana, 1988). This sedimentation was more continuous in the deep basins
76 and discontinuous in the open platforms, with different periods of emersion and erosion, such as in
77 the Middle and Upper Cretaceous and the Paleogene (Zappaterra, 1990). The flexure of the
78 lithosphere coupled with the eastward migration through time, generates a series of foredeep basins
79 parallel to anticlines and filled by terrigenous sediments derived from the progressive erosion of the
80 incipient belt (Ori et al., 1986). The two main detachment levels are the structural elements that drive
81 the fold-and-thrust belt and the foreland area, one at the top of the Triassic succession, within the
82 Triassic evaporites, and one within the Messinian evaporites (Koopman, 1983).

83 During this geodynamic evolution, the marine Jurassic and Cretaceous sedimentary successions were
84 stacked and incorporated in the fold-and-thrust belt and today compose the Apennine orogenic wedge
85 (Cavazza et al., 2004; Carminati and Doglioni, 2012). The result of this geological evolution is the
86 occurrence of fault-related anticlines, with detachment located mainly on the Triassic evaporites, and
87 aligned in the Apennine direction (NW-SE) which constitute, at the present day, the structural setting
88 of the Adriatic domain (Argnani and Frugoni., 1997; Carminati et al., 1998; Castellarin, 2001; Casero,
89 2004; Patacca and Scandone 2004; Bigi et al., 2013; Casero and Bigi, 2013, Cazzini et al., 2015).

90 As evidenced by the intense exploration activity of the oil companies during the 1970s and 1980s,
91 the tectonic and sedimentary evolution generated the conditions for the formation of hydrocarbon
92 fields on both sides of the Adriatic Sea (Casero and Bigi, 2013). At present, hydrocarbons exploration
93 is finished but thanks to this, the area is covered by a quite large (although dated) dataset. This domain

94 has already been identified as a potential area for geological storage of CO₂ (Buttinelli et al., 2011;
 95 Donda et al., 2011; Civile et al., 2013; Volpi et al., 2015, Saftić et al. 2019) for the occurrence of
 96 saline aquifers occurring into the mentioned anticlines and all these studies enable identification of
 97 the calcareous and sandy formations as potential storage reservoirs.

98



99
 100 **Fig. 2.** Area of site screening in the central part of Italy. The location of the identified reservoir is on the offshore of the
 101 Adriatic Sea. The bathymetry is highlighted to show the depth of the seafloor in correspondence of the selected sites. For
 102 the wells is indicated the lithology of the identified saline aquifers and the seismic dataset that allowed the reconstruction
 103 of the structures. The main sources identified in the Geocapacity project (modified by ‘Vangkilde-Pedersen et al., 2009b’)
 104 are indicated with the blue circles, their size depends on the amount of emitted CO₂. (Bathymetry from ‘GeoMapApp –
 105 Ryan et al., 2009’).

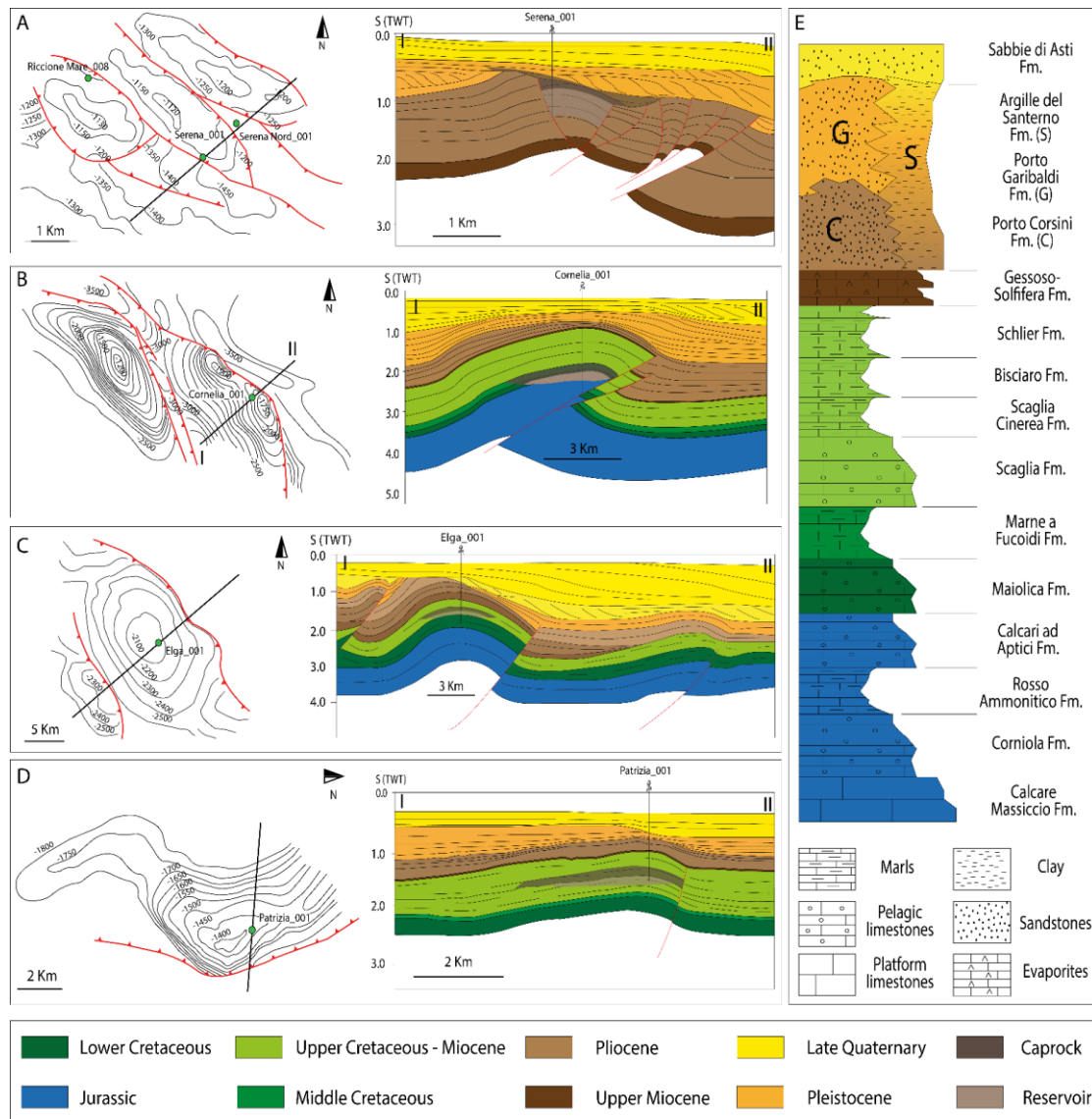
106

107

108 **Data and method**

109 The basis of this work is interpretation of seismic reflection data, analysis of well logs data and
 110 structural maps in the Adriatic Sea, using a combination of public and confidential data. The public
 111 data are available (Fig. 2 and 3) through the ‘Visibility of Petroleum Exploration Data in Italy
 112 (ViDEPi)’ project (Ministry of the Economic Development), a public database deriving from the
 113 petroleum exploration activity conducted in Italy from 1960s up to 2015

114 (<https://www.videpi.com/videpi/videpi.asp>). The public database was supplemented and improved
 115 with seismic reflection datasets from the same areas provided by ENI (National Hydrocarbons
 116 Authority), through a confidentiality agreement.
 117 With the solid framework obtained with seismic interpretation, it was possible to construct 3D
 118 geological models of the saline aquifers hosted into anticlines structures, to obtain an estimate of the
 119 potential volume of CO₂ that can be stored in the selected structures.
 120



121
 122
 123 **Fig. 3** Structural setting of a) Serena, b) Cornelia, c) Elga and d) Patrizia structures identified as possible CO₂ storage
 124 sites in this work (see Figure 2 for location) and stratigraphic log of the Mid Adriatic Sea (d, formation thicknesses are
 125 not in scale). **a)** Isochrone map (in milliseconds of an interval near the top of the ‘Porto Corsini’ Fm., Pliocene) and
 126 interpreted cross section of the Serena structure. This anticline is characterized by several thrust sheet and a very thick
 127 sandy-clay succession, the caprock of the identified saline aquifer is the clay succession of the ‘Argille del Santerno’ Fm.
 128 **b)** Isochrone map (in milliseconds of the ‘Marne a Fucoidi’ Fm., Middle Cretaceous) and interpreted cross section of the
 129 Cornelia anticline. Cornelia is a large anticline with a deep basal detachment, the reference figures indicate the location

130 of the Cornelia_001 well, the level identified as a possible reservoir in the platform limestone formation of ‘Calcare
131 Massiccio’ and the potential caprock in the formation of the ‘Marne a Fucoidi’. **c)** Isochrone map (in milliseconds of the
132 interval of ‘Scaglia’ Fm., Upper Cretaceous) and interpreted cross section of the Elga structure. This structure hosts a
133 suitable reservoir in the fractured calcareous member of the pelagic limestone formation of ‘Scaglia’ and the potential
134 caprock in the formation of the ‘Scaglia Cinerea’. **d)** Isochrone map (in milliseconds of the ‘Scaglia’ Fm., Upper
135 Cretaceous) and interpreted cross section of the Patrizia anticline. The figures indicate the location of the Patrizia_001
136 well and the structural map that shows in this area a main fault plane, linked to the Patrizia anticline. Patrizia is similar to
137 Elga anticline for the structural setting, and it has the same identified formations as the caprock and the reservoir. **e)**
138 Stratigraphy of this sector of the Adriatic domain, the thickness of the formations is not in scale. In the lower part of the
139 log the lithology of the formations is indicated.

140

141 On the basis of various equations, it is possible to estimate the potential volumes (effective capacity),
142 combining the area, thickness, and porosity of the saline aquifer with the N/G ratio and the density of
143 the CO₂ in reservoir conditions (Bachu et al., 2007; Van Der Meer and Yavuz, 2009; Vangkilde-
144 Pedersen et al., 2009a; Goodman et al., 2011). The greater detail and reliability of the data contribute
145 to better definition of capacity and to lowering the cost of using this technology. However, even the
146 theoretical values serve for the authorities in charge and the companies to evaluate the potential of an
147 area and its use. The most used and most efficient equation (1) for calculation of capacity is that
148 established by the USDOE (United States Department of Energy), used for most of the published
149 volume calculations and by the geological storage Atlases (Bradshaw et al., 2011; Wright et al., 2013;
150 Bentham et al., 2014; Riis and Halland, 2014; Ketzer et al., 2015).

151

$$152 \quad MCO_2 = A \times h \times \varphi_m \times \rho_{CO_2} \times E \quad (1)$$

153

154 where:

155 MCO₂ = Mass of CO₂

156 A = Areal extension of the saline aquifer

157 h = Average thickness of the saline aquifer

158 φ_m = Average porosity of the saline aquifer

159 ρ_{CO_2} = Density of CO₂ in saline aquifer conditions

160 E = Storage efficiency factor of the saline aquifer

161

162 In this work, the area and average thickness were substituted by direct estimation of the volume
163 provided by the 3D modelling using dedicated software. The 3D volumes obtained were then
164 populated with the detailed porosity models derived from well log data. To provide the density of
165 CO₂ required in equation (1), the depth of each saline aquifer and the regional geothermal gradient of

166 the Adriatic domain were used (<http://geothopica.igg.cnr.it/>; Bachu, 2000; Kovscek, 2002; Holloway,
167 2005; Suekane et al., 2005; Gough and Shackley, 2006; Ramírez et al.; 2010; Aminu et al., 2017).
168 The petrophysical parameters to populate the 3D geological models were obtained with analysis of
169 the available well logs. Data from four wells, one for each structure, named as the corresponding
170 structure, were used to populate the models. More in detail, the porosity data were obtained from the
171 sonic logs, by transforming the transit times into porosity with the correlation curves between velocity
172 and porosity for carbonates, dolomites, and sandstones (Wyllie et al., 1956,1958,1962; Raymer et al.,
173 1980; Crain, 1986). In this way, a vertical porosity profile with a detail of 10 m was obtained along
174 the well for the saline aquifer thickness interval. These data were upscaled to a 50x50x10 m 3D grid.
175 The method applied to simulate the porosity distribution in the 3D geo-cellular model is Sequential
176 Gaussian Simulation (SGS). The choice of this simulation algorithm is based on the studies by various
177 authors (Journel and Alabert, 1989; Verly, 1993; Al Musawi and Jawad, 2019) who, with several
178 experimental tests of different variogram models, proved that this simulation of porosity distribution
179 is statistically representative. The SGS method is in fact a geostatistical method that is available in
180 Petrel software; it performs a redistribution of the porosity values into the rock volume based on the
181 statistical distribution obtained from the well log analysis. It performs a normal score transformation
182 of the porosity distribution and calculate the probability distribution of porosity values for each node
183 of the grid, starting from a random point and repeated the procedure covering all the volume. The
184 result of the SGS simulation is a statistical distribution of the petrophysical value (in this case
185 porosity) and it is greatly conditioned by the quality and quantity of dataset. It is the most used
186 algorithm for the upscaling of petrophysical properties in saline aquifer modelling as evidenced by
187 the numerous published papers (Guerreiro et al., 2000; Nezhad and Tabatabaei, 2017; Zare et al.,
188 2020; Trippetta et al., 2021). In this work, the main limitation is associated with the use of data from
189 just one well log for each structure; this did not allow the control of the geographical distribution
190 parameter (to simulate a kriged grid) increasing the uncertainties of the procedure (Kavousi and Gao,
191 2013; Xu, 2017).

192 Despite the limitation due to the source of data represented by one well log for each site, the use of
193 the SGS method represents one of the many possible representations of the porosity distribution
194 within the aquifers. This could be improved by multiple repetition of the same method, through a
195 more detailed statistical analysis. Although we are aware of the limit of our SGS simulations
196 determined by the limited data available, we believe that they can still provide a useful indication for
197 example for the expected heterogeneity.

198 However, despite these uncertainties, this method provides a distribution of the measured property
199 even in the case of few data (as in this case) and represent a first approximation of the available pore
200 volume.

201 In fact, the distribution of vertical and horizontal porosity within the geocellular model also results in
202 a pore volume value, which can be representative of the theoretical porosity of the aquifers. A similar
203 single pore volume value can be obtained simply by multiplying the gross rock volume by the average
204 porosity from each well; in this light, the advantage of using the SGS simulation is to obtain a
205 representation of the heterogeneity (statistical) of the porosity in the aquifers.

206 A realistic value of the pore volume and the distribution of porosity is achieved through the choice of
207 factors called variograms, which drive the possible realizations of the cell models. Variograms control
208 the spatial variance of properties that can be attributed to a distribution model. In the case of models
209 referring to a geological formation, these will drive heterogeneities in the distribution of properties
210 such as facies, porosity or permeability, and fluids. There are some parameters that must be defined
211 to distribute these properties such as angles, ranges, anisotropies, means and standard deviation.

212 Behind the choice of the various parameters that govern the variograms there can be different
213 approaches, from well data to outcrop analogues. For the population of the aquifers in this work we
214 adopted parameters on the base of geological constraint described in detail in the next paragraph.

215 From equation (1), once the pore volume (3D volume $\times \phi_m$) is obtained from the geo-cellular model,
216 the CO₂ density (ρ_{CO_2}) should be estimated at the saline aquifer condition (Doughty et al., 2001;
217 Bachu et al., 2007; Vangkilde-Pedersen et al., 2009a; Goodman et al., 2011).

218 The main factors that influence the density of CO₂ are pressure and temperature. Therefore, when
219 calculating the density of CO₂, the effective pressure and temperature of the saline aquifer must be
220 defined. According to Terzaghi (1925; 1936) the effective pressure of the saline aquifer is calculated
221 by:

222

$$223 \sigma_{\text{effective}} = \sigma_{\text{lithostatic}} - \sigma_{\text{pore}} \quad (2)$$

224

225 where $\sigma_{\text{lithostatic}}$ = pressure of the water column (if the saline aquifer is offshore) plus the head of the
226 rock column. the pressure of the water column depends on the density and depth of the sea water as
227 well as the density and thickness of the rocks above the reservoir (Carrozzo et al, 1990; Venisti et al.,
228 2004); σ_{pore} is the pore pressure within the saline aquifer and depends on the hydrodynamic condition
229 of the saline aquifer itself; $\sigma_{\text{effective}}$ represents the real pressure state of the saline aquifer (Avseth,
230 2010; Smith et al., 2011).

231 Pore pressure data were obtained from public sources (wells from ViDEpi), and estimation of pressure
232 in depth was performed using the Petroleum Systems Modeling Software PetroMod. Pore pressure
233 was modelled with 1D models considering only pure hydrostatic conditions.

234 The storage efficiency factor (E) is one of the most important variables for calculation of storage
235 capacity. It is derived from many site operations and dynamic or numerical simulation, such as the
236 Monte Carlo simulation (NETL, 2008), during injection. The storage efficiency factor in saline
237 aquifers is based on a series of parameters and components that represent different physical limits
238 and barriers that prevent the injected CO₂ from filling the entire pore volume in a certain saline aquifer
239 or basin. These limits are dependent on the total volume, the total porosity, the effective porosity, and
240 the permeability, so the reason for including the storage efficiency factor in Eq.1 is to quantify the
241 volume that can be used to store and inject CO₂. This coefficient is not unique, it varies according to
242 many factors such as net to total area, fraction of an area with suitable formation present, net to gross
243 thickness, fraction of geological formations with minimum petrophysical characteristics suitable for
244 injection, ratio between total and effective porosity, areal displacement efficiency, geological
245 formation heterogeneity, presence of fault, vertical displacement efficiency, gravity, capillarity, brine
246 salinity, buoyancy, microscopic displacement efficiency, water saturation of the aquifer (NETL,
247 2006, 2008; IEA GHG, 2009). These factors are grouped into a single parameter called Storage
248 Efficiency Factor which defines the percentage of the pore volume that can be exploited, since the
249 inclusion of all these parameters within E considers all the possible variables. The variability of the
250 values of the different parameters indicated by the different authors is an approximation; it is intended
251 to be representative for various structural arrangements, depositional systems, and lithological
252 characteristics that have different boundary conditions.

253 Considering all these variables, the proposed range for the storage efficiency factor for open aquifers
254 is between around 1% and 4%, based on the type of saline aquifer (Doughty et al., 2001; Bachu et al.,
255 2007;2015; Vangkilde-Pedersen et al., 2009a; Goodman et al., 2011). In closed structures, such as
256 anticlines or domes, the storage efficiency factor assumes values between 1% and 20% (Gorecki et
257 al., 2009; Vangkilde-Pedersen et al., 2009a; 2009b; Marek et al., 2011; Knopf and May, 2017). The
258 higher value reflects the fact that in the anticlines the mechanism of structural confinement plays a
259 very important role, which significantly increases the trapping efficiency and the value of E. In this
260 work values of 7% for fractured pelagic carbonates, of 10% for fractured platform carbonates and
261 13% for sandstones are considered. The choice of the E value for pelagic and platform limestones is
262 in accordance with the storage efficiency factors proposed for saline aquifers identified in closed
263 structures (Gorecki et al., 2009; Marek et al., 2011; Knopf and May, 2017); in the case of Serena
264 anticline, which hosts a siliciclastic reservoir E should be higher, close to about 18%. The choice of

265 a lower value is due to the fact that Serena is fault bordered and injection at high pressure could cause
266 a reduced displacement of the native fluids, thus limiting the storage efficiency during the injection
267 phase.

268 These E values, adopted from the previously mentioned studies, are based on different lithologies and
269 reservoir boundary conditions and can be corrected and specified with future detailed research. The
270 importance of the lateral heterogeneity of the aquifers and its behavior, the interaction with capillary
271 pressure and the possible lateral migration of CO₂ can affect - in most cases reduce - the effective
272 storage capacity and efficiency of the geological formations (Williams et al., 2013).

273

274 **Structures**

275 Of the areas and structures (Donda et al., 2011; Civile et al., 2013) identified as possible storage sites
276 in the Adriatic offshore, four structures largely covered by ample datasets are chosen. These structures
277 (Fig. 2) are located offshore in the Northern-Mid-Adriatic Sea: Cornelia, Elga and Serena anticlines
278 in the north and Patrizia anticline in the centre Adriatic Sea All of them have already been identified
279 as excellent targets for CO₂ storage in previous studies on both the regional (Buttinelli et al., 2011;
280 Donda et al., 2011; Civile et al., 2013) and local scale (Cappelletti et al., 2012; Teatini et al., 2014).
281 Figure 3 shows the geological setting and the stratigraphy of Cornelia, Patrizia, Serena and Elga
282 anticlines, the latter being very similar to the Patrizia structure both in the setting and the lithology.
283 The Serena anticline (Fig. 3a) is in the northern Apennines offshore, in an area where the Plio-
284 Quaternary siliciclastic succession is involved in thrusting. It is characterised by several thrust sheets
285 that affected the Pliocene deposits, composed of a thick sandy-clay succession with marked lateral
286 facies heterogeneity. The saline aquifer of the Serena anticline is recognized in the thick Pliocene
287 siliciclastic sequence on the top of the Adriatic Mesozoic formations, the Porto Corsini Formation
288 delimited at the top by tens of metres of clay succession of the 'Argille del Santerno' Formation (Fig.
289 3e) (Castellarin, 2001; Patacca and Scandone 2001; Artoni, 2013).

290 Cornelia is a thrust-related fold (Fig. 3b) in the northern-Apennines offshore, in an area that includes
291 many compressive structures linked to as many reverse faults. In the case of Cornelia, the main thrust
292 fault plane splits into another minor plane cutting the forelimb of the anticline. The anticline is
293 composed of the Mesozoic succession, covered by the Plio-Quaternary siliciclastic facies (Casero and
294 Bigi, 2013). For the Cornelia anticline, the target reservoir is the 'Calcare Massiccio' Formation a
295 thick Jurassic formation consisting of fractured and dolomitized platform limestones. The porosity is
296 due to fracture intensity and dolomitization, two excellent properties for a site in view of the
297 possibility of storing carbon dioxide. The caprock is identified in the 'Marne a Fucoidi' Formation
298 (equivalent), composed of calcareous micrites and marl intercalations (Fig. 3e). This formation is

299 generally recognized by oil exploration companies as a very good seal in the Adriatic area. In this
300 structure, the base of the reservoir is around 2700 m in depth, while the base of the caprock
301 approximately 200 m above.

302 Elga (Fig. 3c) is a fault-related anticline in the offshore of northern Apennines, close to the anticline
303 of Cornelia. In the case of the Elga structure, the formations identified as reservoir and caprock are
304 the Scaglia Formation and the Scaglia Cinerea Formation, respectively. These formations are the
305 same as can also be recognised in the case of the for Patrizia anticline (Fig. 3d), located further south;
306 the only difference lies in the depth of these formations, greater in Elga. These structures are mainly
307 composed of the Cretaceous carbonate succession and are covered by the Plio-Quaternary siliciclastic
308 sequence. The potential reservoir for the CO₂ storage is the calcareous member of the ‘Scaglia’
309 formation, composed of fractured pelagic limestones; more in detail, this is made up by calcareous
310 layers and marly intervals with a high level of fracture intensity on outcropping analogue (Tavani et
311 al., 2008; Petracchini et al., 2012). The Patrizia reservoir has a thickness of around 100 m, while in
312 the Elga anticline the thickness is around 270 m. A very good factor in these anticlines is the large
313 areal extension, resulting in the very large potential reservoir volume of the structures. The caprock
314 is the Scaglia Cinerea Formation, an alternation of marls and calcareous marls, for about 250 m of
315 thickness (Fig. 3e).

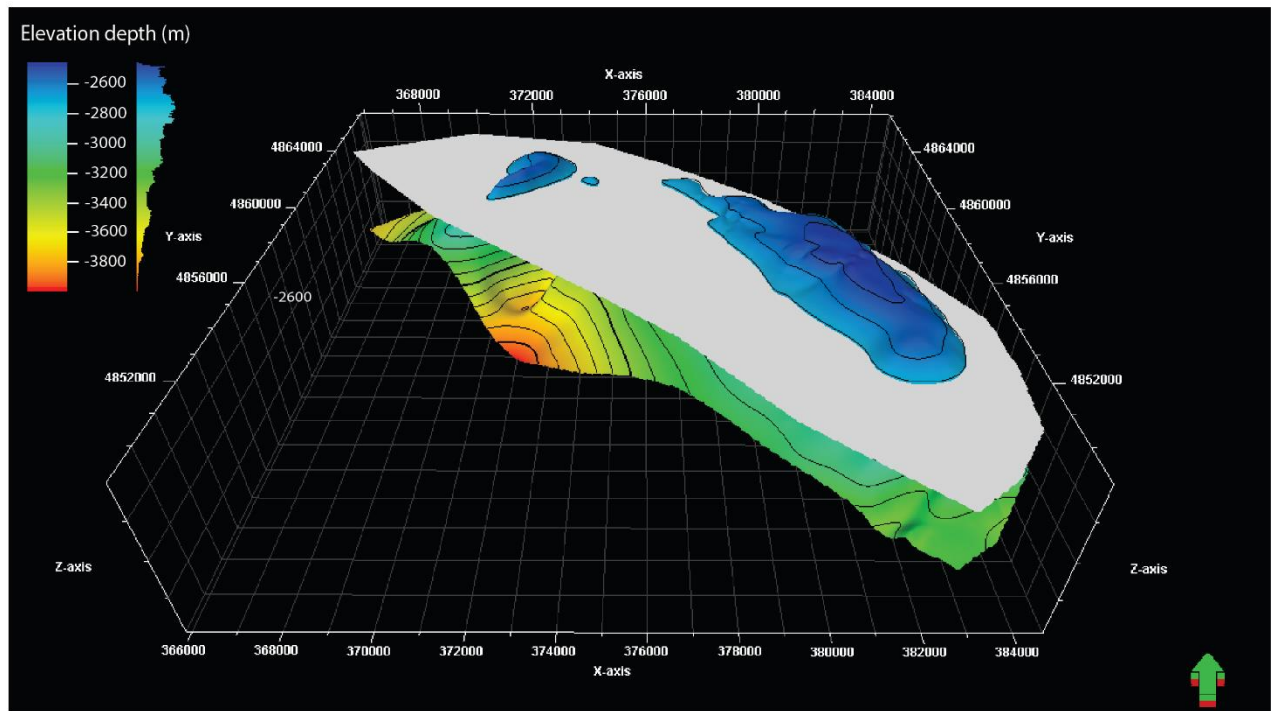
316

317 **Saline aquifer volume calculation**

318 The 3D geological models are generated from a dense 2D seismic lines interpretation framework,
319 with an average line spacing of about 600 m, which is the basis for the volumetric modelling of the
320 saline aquifers, subsequently populated with the porosity derived from well data.

321 In the Cornelia, Patrizia and Elga structures the maximum depth of the exploitable saline aquifer
322 volume is determined above the depth at which the saline aquifer formation is in contact with the
323 thrust fault; in this way, the role of the fault as a potential conduit is avoided. In fact, since its
324 behaviour is unknown, this choice considerably reduces the risk of leakage through the fault. For
325 these three structures (Fig. 4), the top surface of the saline aquifer formations (z-values surface) and
326 a flat ‘artificial’ surface (in white) are modelled to identify a “spill-point” which is limited by a fault
327 at that depth, assumed to be the maximum depth for feasible CO₂ injection. This procedure is applied
328 to all carbonate saline aquifers, while in the siliciclastic saline aquifer of Serena the maximum
329 exploitable depth was taken to be that of the bottom of the well itself.

330



331

332

333 **Fig. 4.** 3D modelling arrangement for the determination of the exploitable part of the saline aquifer formation. This model
 334 refers to the Cornelia anticline. The colour-scale surface represents the top of the formation with good reservoir
 335 characteristics, whereas the white flat surface represents the lower depth for the storage interval. The blue-scale surface
 336 of the formation above the flat surface is the interval in the right depth range, therefore exploitable for storage.

337

338 In Cornelia, the base depth of the reservoir is 2700 m, and it was chosen on the basis of the data
 339 analysis of the Cornelia 001 well, which shows good porosity and fracture intensity conditions down
 340 to this depth. For Elga the basal limit is 2350 m, corresponding to the base of the saline aquifer
 341 formation, whereas for the Patrizia structure, the basal limit is the maximum depth of 1648 m.

342 In the case of Serena, the reservoir is bordered laterally by two faults, so an evaluation of the
 343 behaviour of these faults is required. However, it is difficult to determine their behaviour as no direct
 344 data are available for this kind of evaluation, we lack detailed stratigraphy of the siliciclastic
 345 succession in the hanging wall and in the footwall of the faults, as well as data on the amount of the
 346 offset of the faults themselves (Yielding et al., 1997; Freeman et al., 1998; Harris et al., 2002). The
 347 only indication on fault behaviour in the Serena structure can come from the occurrence of fluids, just
 348 water in the Serena well, detected in other wells located in adjacent sectors for the same stratigraphic
 349 interval. In fact, in well Serena Nord 001 and Riccione Mare 008 (Fig. 3a), that are located
 350 respectively at a distance of about 1.1 km and 5 km from the Serena well, for the same stratigraphic
 351 interval, that is at depth between 1084 and 1300 m, the report of the wells indicates that there are
 352 formation water and the occurrence of gas, and this difference is probably linked to the lack of
 353 communication between the wells. This observation leads to the assumption that essentially these

354 faults act as a barrier and does not favour fluid migration. Of course, the seal effect is also connected
355 with the capillary pressure exerted by the supercritical CO₂ once injected into the saline aquifer, but
356 the observed distribution of water can also support the occurrence of a sufficient threshold of capillary
357 pressure.

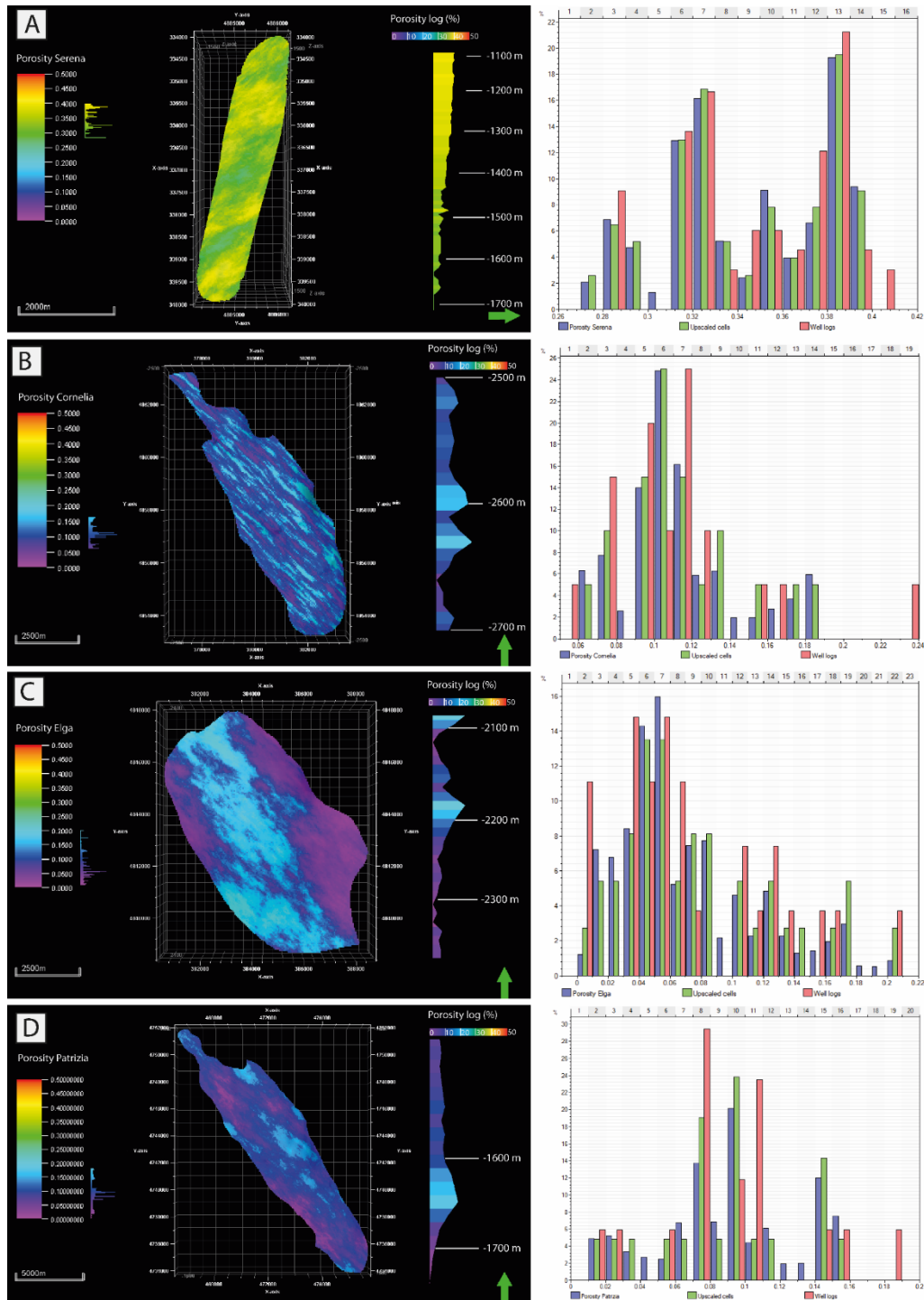
358

359 **3D models**

360 The frequency distribution logs of porosity values shown in Fig. 5, is obtained from sonic log analysis.
361 The composite logs available for the analysed wells also comprise the resistivity and the spontaneous
362 potential logs, as well as the description of several core samples at different depths within the saline
363 aquifer interval. In the case of the Patrizia well, where the potential reservoir is in the Scaglia
364 Formation, the occurrence of fractures is described in one core sample, whereas no data are available
365 for the Elga well. The description of lithologies in the Cornelia well indicates the occurrence of
366 fractures in both the calcareous and dolomitic reservoir interval, whereas there is no indication of
367 fracture intensity for the Patrizia well. For these reasons, the porosity distribution obtained from sonic
368 log can be considered as representative of both the primary and secondary porosity without any
369 possibility to distinguish between them. Of course, at least in the case of the Cornelia and Patrizia
370 wells, some of the porosity values measured are due to the occurrence of fractures but on the evidence
371 of the above-mentioned dataset it is not possible to define the fracture intensity contribution to the
372 total porosity.

373 Considering the range and average values, the highest porosity values concern the siliciclastic saline
374 aquifer of Serena (Fig. 5a) with a range from 27% to 40%. For the carbonate saline aquifer, the values
375 are generally lower: the platform limestone formation of the Calcare Massiccio Formation of the
376 Cornelia anticline shows porosity ranging between 5% and 24% (Fig. 5b), whereas Elga (Figs. 5c,
377 5d) has porosity values ranging between 3% and 16%, and between 1% and 18%, for Patrizia. Despite
378 these average values, the Scaglia Fm shows thin intervals with slightly higher values, even up to
379 porosity greater than 30%; these levels correspond to calcareous turbidites deposits intercalated
380 within the pelagic mudstones and /or to dolomitic levels.

381 For the choice of the parameters of the variograms in all the structures, an angle of 135 ° with respect
382 to the north was set, therefore NW-SE, since the lateral heterogeneity, linked to both the depositional
383 system of the formations and the current geological structure, follows the orientation of the Apennine
384 chain. For the property values, the mean, and standard deviation, a 'from upscaled log' distribution
385 was used, which then follows the well log values. In this way, these aquifers show several differences
386 in the spatial ranges of the internal anisotropies of the aquifers, which depend on the different
387 formations.



388

389

390 **Fig. 5.** 3D petrophysical models of the exploitable part of the saline aquifer. For each storage site model is shown the data
 391 relative to the porosity frequency and to porosity log values in depth. The histograms are included to illustrate the
 392 statistical distributions of the porosity for each structure, derived from upscaled log and upscaled cells. These histograms
 393 represent the relationship between porosity values and percentage of the total volume. **a)** Serena structure; **b)** Cornelia
 394 anticline; **c)** Elga structure; **d)** Patrizia anticline (See Fig. 2 for the location).

395

396 The Serena anticline hosts a siliciclastic reservoir that was deposited in a context of thrust-top basin
 397 (Ori et al., 1986), thus a basin that received sediment flows from an eroding chain behind it. The

398 heterogeneity of the sands is therefore oriented in the direction of the advancing chain and the basin
399 has an elongated shape in the NW-SE direction of the order of a kilometre, and a lateral variation in
400 a range between 300 and 400 m (Ghielmi et al., 2013). The range of anisotropies chosen in this case
401 is therefore 1000 x 350 m, in accordance with studies on the sedimentology of these deposits. The
402 Cornelia structure hosts a saline aquifer composed of platform limestones from the Calcare Massiccio
403 formation. The platform limestones generally show a great lateral heterogeneity, deriving from the
404 facies, the depositional system and the nature of the carbonate platforms which is very dynamic. The
405 geometry of the anisotropies was strongly elongated to fit with the facies in the carbonate systems
406 (Fig.5b) (Brigaard et al., 2014), and the range chosen is 1000 x 150 m, to represent even the structural
407 control of the anticline.

408 For the structures of Elga and Patrizia the saline aquifers have been identified in the Scaglia
409 Formation, a formation composed of carbonate pelagic deposits. This formation consists of pelagic
410 mudstones mainly composed of planktonic foraminifera and carbonate mud, except in the areas close
411 to the platforms where carbonate calcarenite flows are present (Colacicchi et al, 1986; Fabbi et al.,
412 2016). Apart from these latter deposits, the Scaglia formation is almost totally homogeneous laterally,
413 so the ranges chosen for the anisotropies are very large, about 7000 x 3000 m, and are intended to
414 represent the lateral variability related to the anticline structuring.

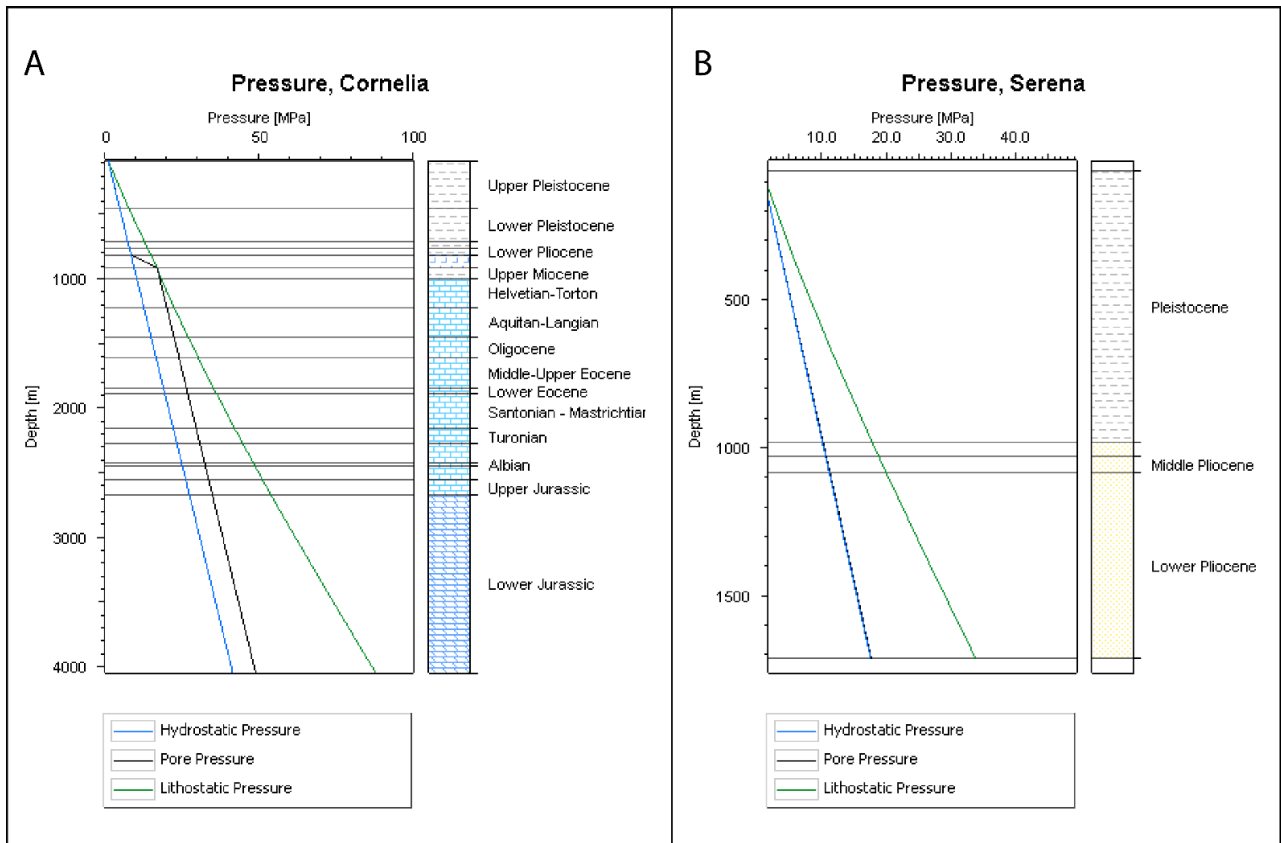
415

416 **CO₂ density estimation**

417 Calculation of the potential capacity of the structures considered called for definition of average
418 values for porosity and its distribution and CO₂ density. For the latter, the effective pressure and
419 temperature in the saline aquifer has been reconstructed.

420 The reconstruction of the pressure-depth trend was performed using Petromod software by
421 Schlumberger, adopting 1D models. It could be improved by introducing analysis in 2D and 3D,
422 which requires data on the stress generated by the occurrences of faults and the pressure distribution
423 under salt layers. In this case, only the 1D reconstruction was performed, and it revealed two different
424 scenarios in the wells analysed (Fig. 6). The main problem resulting from the lack of the spatial
425 relations data is that, in this condition, it is not possible to determine the outflow pressure below the
426 potential impermeable layer, but only to define the occurrence of an overpressure. Moreover, we were
427 unable to include the tectonic stress from possible surrounding faults (at Serena) when the modelled
428 pressure was too low. The pressure information was drowned from the Schlumberger DST (drill stem
429 test) data as shown in the composite logs of the wells analysed, and in some cases confirmed by the
430 mud weight used while drilling (Fig. 7).

431



432

433

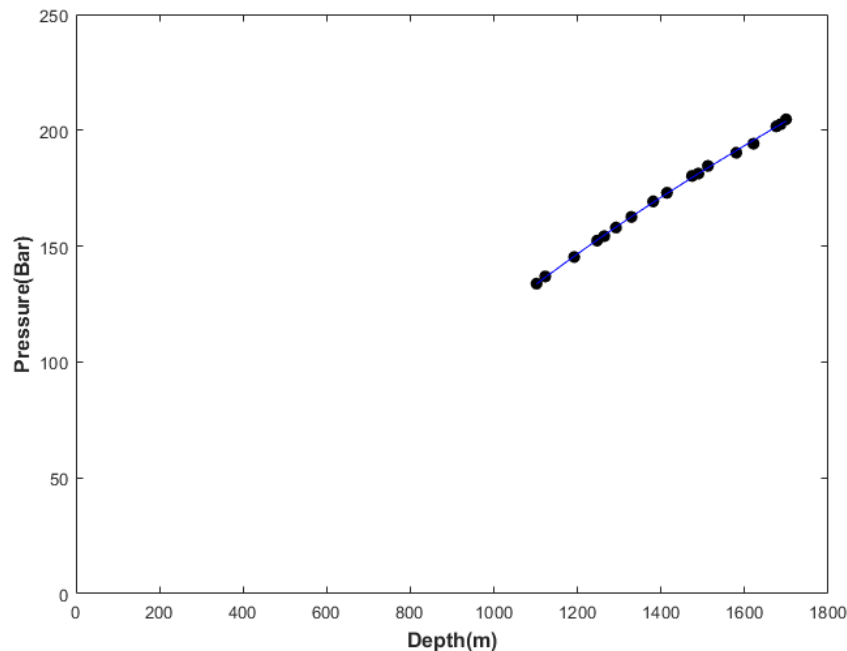
434 **Fig. 6. a)** Salt and **b)** non-salt pressure modeling scenarios. In the salt scenario the presence of the Messinian evaporites
 435 generates an abrupt increase of the pore pressure (black line) inside this interval, respect to the linear increase of the
 436 hydrostatic pressure. In the non-salt scenario, the behaviour of the pore pressure is the same of the hydrostatic pressure
 437 for the absence of a low-permeability interval that acts as a seal and considerably increase the pore pressure. This mean
 438 that in the salt scenario the pore pressure is higher than the hydrostatic pressure, while in the non-salt scenario the
 439 pressures have the same value.

440

441 The PetroMod modelling shows a clear difference between the linear increase of lithostatic and
 442 hydrostatic pressure and the non-linear increase of pore pressure. Overpressure build-up zones in
 443 some of the wells analysed is generated by the hindering of the normal compaction process due to the
 444 low permeability of the Messinian evaporites levels in the upper part of the well (Bertoni
 445 and Cartwright, 2015). In fact, this high efficiency evaporitic seal acts as a barrier to fluids and
 446 generates an abrupt increase in the pressure of the pores in the intervals beneath it (Nashaat, 1998)
 447 (Fig. 6). This leads to the presence of a salt-scenario and a non-salt scenario in wells analysed
 448 resulting in different pore pressure distribution. The consequence is a different calculation of the
 449 resulting effective pressure of the saline aquifer as a function of Eq. (2).

450 In a salt-scenario (Fig. 6a), as in the case of the Cornelia well, the pore pressure increase is greater
 451 than the hydrostatic pressure increases due to the presence of salt, so the resulting effective pressure
 452 is in accordance with Eq. (2), because the pore pressure value is different from the hydrostatic

453 pressure value. In a non-salt-scenario, as in the case of the Serena well (Fig. 6b) the increase in pore
454 pressure will be equal to the increase in hydrostatic pressure, so the values are the same and the
455 resulting effective pressure is the difference between lithostatic pressure and hydrostatic pressure.
456



457
458 **Fig. 7.** Graphical plot showing the measured pressure data (from the DSTs) and depth in the Serena well.
459

460
461 In the Patrizia well, the interval analysed is from 1558 m to 1648 m, the well bottom. The well
462 pressure data are drawn from formation testing, and the pressures noted in the interval were 180.9
463 kg/cm^2 (177.4 bar). This indicates slight overpressure, even more in shallower layers, whereas in the
464 target interval from 2080 to 2350 m of depth in the Elga well, the pore pressure is near hydrostatic,
465 ranging from 208 to 234 Bar (212-238 kg/cm^2). Although this well, too, had salt intervals in the
466 Messinian formation in the upper part, the pressure in the bottom layers is still hydrostatic, suggesting
467 the occurrence of a large aquifer, which is favourable for CO_2 storage. The effective saline aquifer
468 pressure together with the temperature were used to calculate the CO_2 density conditions in the
469 reservoir (Table 1). The Serena well crosses the saline aquifer interval from 1084 m to 1748 m. At
470 1102 m the pressure is 131.2 bar and at 1676 m it is 197.8 bar, so the pressure gradient factor is from
471 1.3 to 1.203. The interval of interest in the Cornelia well is from 2500 to 2700 m; due to the Messinian
472 evaporites the pressure modelling shows a slight overpressure with gradient of 1.2 (Fig. 6, Table1).
473 Temperatures of the saline aquifers were taken from the portal of the Geothopica Project
474 (<http://geothopica.igg.cnr.it/>), a public national database that incorporates the subsurface data, the hot
475 springs, gas, geothermal points, wells, isotherms, and the heat flow in Italy. In our case, for the

476 Cornelia, Elga and Patrizia wells, available temperatures of 341.15 K, 339.15 K and 313.15 K
 477 respectively were measured in the well during drilling. For Serena, the Geothopica database indicates
 478 the target depth temperature of 313, 15 K, derived from the geothermal gradient.
 479 With pressure and temperature values it is possible to calculate the density of the CO₂ for the injection
 480 in reservoir conditions. This calculation is very important because it will also serve for guidance in
 481 many of the decisions that will be made during injection. For the estimation of CO₂ density in this
 482 work the calculator of the Penn State Energy Institute - College of Earth and Mineral Sciences was
 483 used ([http://www.energy.psu.edu/tools/CO2- EOS/](http://www.energy.psu.edu/tools/CO2-EOS/); Span and Wagner, 2006).

484

Structures	Reservoir Volume (m ³)	Pore Volume (m ³)	Effective Pressure (Bar)	Effective Temperature (K)	CO ₂ density (kg/m ³)	Storage efficiency factor (%)	CO ₂ storage capacity (Mtons)
Serena	3476 x 10 ⁶	1082 x 10 ⁶	206,13	313,15	864,06	13	119
Cornelia	3308 x 10 ⁶	337 x 10 ⁶	368,27	341,15	845,4	10	28
Elga	10331 x 10 ⁶	659 x 10 ⁶	302,37	339,15	807,02	7	37
Patrizia	10880 x 10 ⁶	914 x 10 ⁶	178,7	313,15	818,16	7	56

485

486 **Table 1.** Results of static capacity estimations for the identified reservoirs in the Mid Adriatic Sea.

487

488

489 Results

490 Table 1 shows the results relating to the estimation of the storage capacity for the potential structures
 491 identified. All the parameters used for this calculation are indicated for each structure, including the
 492 total volume of the saline aquifer, the porosity, and the effective pressure in the conditions of the
 493 reservoir, obtained by the difference between the lithostatic and pore pressure, the temperature from
 494 the well data and the information relating to the density of CO₂ in the injection conditions. The storage
 495 efficiency factors, adopted for each structure are in accordance with Vangkilde-Pedersen et al.
 496 (2009a) and Knopf and May (2017). Serena structure shows a potential storage capacity of 120 Mt,
 497 whereas the dolomitized saline aquifer of Cornelia, shows a potential exploitable volume of about 30
 498 Mt; the pelagic limestones of the Elga and Patrizia structures have a storage capacity value of 43 and
 499 103 Mt, respectively.

500 Several studies have been conducted on macro-areas and on a regional scale to evaluate the storage
501 capacity of the Italian territory (Buttinelli et al., 2011; Donda et al., 2011; Moia et al., 2012; Civile et
502 al., 2013; Volpi et al., 2015). Although the database used by these Authors is essentially the same as
503 used in this work, the capacity presented in these studies has values considerably higher than those
504 obtained by this work. These differences are mainly due to decisions adopted during calculation
505 procedure and to the values of the efficiency factors. In fact, previous works calculated volumes
506 without a 3D reconstruction, using structural maps and formation thickness, and adopting average
507 porosity and permeability values, instead of the upscaling approach used in this work thanks to the
508 SGS simulation. One of the main factors was the definition of the bottom of the reservoir, that has
509 been identified by using a flat ‘artificial’ surface to represent the base of the aquifer controlled by the
510 structural traps represented by the geometry of the anticline. In Cornelia and Patrizia this flat surface
511 represents the base of the limb of the anticline, while in Elga the base derives from the ‘artificial’ flat
512 surface and the top of the ‘Marne a Fucoidi’ Formation, immediately below the ‘Scaglia’ Formation,
513 since the ‘artificial’ surface cuts through the underlying formation. In Serena it is not necessary to
514 define this surface because from the seismic interpretation it was possible to reconstruct three-
515 dimensionally the base surface of the structure, located within the established depth range.
516 The efficiency factors used in this work are very conservative and greatly affect the results obtained;
517 this can be deduced from the values of the theoretical capacity- which are more comparable with
518 those of the previous works. The next step will be dynamic simulation of CO₂ injection into the saline
519 aquifer; in this way a more comprehensive description of saline aquifer behaviour can be defined,
520 and the matched capacity can be calculated.

521

522 **Discussion**

523 In this work, we focus on the offshore of the Adriatic Sea, one of the areas in the Mediterranean
524 domain considered suitable for CO₂ storage; oil and gas exploration has been conducted there, mainly
525 during the 1970s and 1980s. Evaluating the capacity of an area already extensively studied by oil/gas
526 exploration has several advantages. The information already acquired on the geometric and
527 petrophysical characteristics, together with the pre-existing infrastructure, and the proven fact that
528 the geological formations targeted have already hosted fluids, all suggest that they will be able also
529 to trap CO₂. Once a saline aquifer has been considered a good candidate for geological storage, the
530 next step and one of the most important is the estimation of the geological storage capacity, or the
531 physical limit of CO₂ that the saline aquifer can host. This value must be established to determine the
532 maximal volume of CO₂ that theoretically can be used in the injection phase. The 3D modelling

533 approach is used to obtain more accurate storage capacity estimates for the potential structures
534 identified; in this way we can arrive at more realistic definition of the potential for the studied area.
535 The effective storage capacity of four potential reservoirs for geological storage in the Adriatic Sea
536 has been estimated. Two of these saline aquifers have been identified in the member of fractured
537 limestones of the 'Scaglia' formation, and in the anticlines of the Patrizia 001 and Elga 001 wells. A
538 reservoir has been identified in the formation of the dolomitized platform limestones of the 'Calcare
539 Massiccio' Formation in the Cornelia anticline, while further to the North, a saline aquifer in the Plio-
540 Quaternary siliciclastic sequence has been identified through the analysis carried out in the structure
541 crossed by the Serena 001 well. Finally, the storage capacities are estimated using different storage
542 efficiency factors, applying the more realistic E value for the identified saline aquifers, based on
543 depth, facies, and exploration level.

544 The methodology explained here has been applied to a public database obtained from the oil and gas
545 exploration in the area. Certainly, this dataset allowed us the definition of the range of values of the
546 main parameters and obtain the potential for the theoretical and effective capacity estimates for almost
547 every structure that has already been drilled, which is important for estimation of the CO₂ geological
548 storage as a novel national resource. On the other hand, regional seismic grids, and vintage well data
549 are frequently insufficient to reach more detailed evaluations, which in any case would require more
550 complete and dedicated studies. In this way the results from studies like the present one can help in
551 drafting the targeted exploration projects that will catalyse the developments, i.e. attract investments.
552 CO₂ injection in carbonate successions has been extensively studied in the literature and
553 experimentally, and it is well known that this type of injection has many positive aspects. The
554 carbonate formations provide favourable conditions of confinement because the fracture networks
555 developed can be exploited both as networks for diffusion of the plume and as a volume itself.
556 Furthermore, the carbonate facies, through the dissolution processes linked to the pH variation, can
557 generate a greater volume for the storage of carbon dioxide (Luquot and Gouze, 2009). Some studies
558 also focus on the possible negative effects that could result from brine acidification (Deng et al., 2015;
559 Peng et al., 2016), but these studies conclude that acidification has very little effect in saline aquifer
560 conditions and one of the major effects is improved permeability, a positive factor in the CO₂ storage
561 process.

562 In the geological storage of CO₂, certain aspects need particular consideration, since the aim of this
563 technology is to inject the largest possible amount of fluid without compromising the integrity of the
564 saline aquifer. For this reason, the most constraining limit chosen in this work is the depth of the
565 reservoirs. A storage site should usually be at a depth between 800 m and 2500 m, to have a balance
566 between the volume of the CO₂ injected and the storage costs, i.e. for the operation to be economically

567 viable. This depth reaches 2700 m in favourable conditions, such as the presence of the already
568 existing infrastructure that can be used to reduce the capital investment, and also if the saline aquifer
569 facies is prone to the storage or has a high level of fracture intensity, which would significantly
570 increase injectivity.

571

572 **Conclusions**

573 For characterization of the storage sites, the first phase is seismic interpretation of the structures
574 chosen as possible storage targets. With the combination of public (ViDEPi) and confidential (ENI)
575 data, a solid seismic interpretation framework of four structures (Cornelia, Elga, Patrizia and Serena)
576 was constructed, and served as the basis of 3D modelling in Petrel. All these structures are anticlines,
577 trending mainly NW-SE, located in the northern and central Adriatic Sea. The total volumes obtained
578 populated with the distribution of porosity values derived from sonic log analysis, and the total pore
579 volume arrived were combined with the CO₂ density achieved using temperatures and pressure in
580 reservoir conditions. Theoretical and effective capacity values were then calculated using eq. (2). The
581 obtained values, showed in table 1, are more conservative than those previously published, although
582 the datasets used are essentially the same. This is due to the constraints defined specifically from each
583 structure, and the use of the 3D model, which allows for more precise definition of the available
584 volumes.

585 The saline aquifers analysed in this work are strategically located and have enough storage capacity
586 to be considered in hypothetical CCS projects. Moreover, the occurrence of numerous sources of CO₂
587 along the Adriatic Sea coastline and in the Po Plain (Fig. 2), identified in the final report of the
588 GeoCapacity project (Vangkilde-Pedersen et al., 2009b) makes these saline aquifers attractive storage
589 option, due to the proximity to CO₂ emission points that reach up to 10 Mt/year.

590

591

592 **Acknowledgments**

593 Special thanks to Eni E&P for the kindly sharing private data essential for the realization of this work.
594 We thank Schlumberger S.p.A for the academic license of the Petrel E&P software platform (*Mark
595 of Schlumberger). Thanks to the suggestions of editor and reviewers that strongly improved the
596 quality of this paper.

597

598

599

600

601 Al Musawi, J. M., & Al Jawad, M. S. (2019, July). Study of different geostatistical methods to model formation porosity
602 (Cast study of Zubair formation in Luhais oil field). In IOP Conference Series: Materials Science and Engineering (Vol.
603 579, No. 1, p. 012031). IOP Publishing.

604

605 Aminu, M. D., Nabavi, S. A., Rochelle, C. A., Manovic, V. 2017. A review of developments in carbon dioxide storage.
606 *Applied Energy*, 208, 1389–1419, doi:10.1016/j.apenergy.2017.09.015

607 Argnani, A., Frugoni, F. 1997. Foreland deformation in the Central Adriatic and its bearing on the evolution of the
608 Northern Apennines. *Annali di Geofisica*, **40**, 771–780.

609 Artoni, A. 2013. The Pliocene-Pleistocene stratigraphic and tectonic evolution of the Central sector of the Western
610 Periadriatic Basin of Italy. *Marine and Petroleum Geology*, **42**, 82–106, doi:10.1016/j.marpetgeo.2012.10.005

611 Avseth, P. 2010. Explorational Rock Physics – The Link Between Geological Processes and Geophysical Observables.
612 *Petroleum Geoscience*, 403–426, doi:10.1007/978-3-642-02332-3_18

613 Bachu, S. 2000. Sequestration of CO₂ in geological media: criteria and approach for site selection in response to climate
614 change. *Energy Conversion and Management*, **41**, 953–970, doi:10.1016/s0196-8904(99)00149-1

615 Bachu S., Bonijoly D., Bradshaw J., Burruss R., Holloway S., Christensen N.P. 2007. CO₂ storage capacity estimation:
616 methodology and gaps. *International Journal of Greenhouse Gas Control*, **1**, 430–443.

617 Bachu, S. 2015. Review of CO₂ storage efficiency in deep saline aquifers. *International Journal of Greenhouse Gas*
618 *Control*, **40**, 188–202. doi:10.1016/j.ijggc.2015.01.007

619 Bentham, M., Mallows, T., Lowndes, J., Green, A. 2014. CO₂ STORAge evaluation database (CO₂ Stored). The UK's
620 online storage atlas. *Energy Procedia*, **63**, 5103-5113.

621 Berenblyum, R., Audigane, P., de Dios, J. C., Gastine, M., Hladik, V., Koenen, M., Wildenborg, T. 2018. Enabling
622 Onshore CO₂ Storage in Europe (ENOS): First Outcomes. In 14th Greenhouse Gas Control Technologies Conference
623 Melbourne (pp. 21-26).

624 Bernoulli, D. 2001. Mesozoic-Tertiary carbonate platforms, slopes and basins of the external Apennines and Sicily. In:
625 Vai, G.B., Martini, I.P. (eds.) *Anatomy of an Orogen: the Apennines and Adjacent Mediterranean Basins*. Kluwer
626 Academic, London, 307–326.

627 Bertoni, C., Cartwright, J. 2015. Messinian evaporites and fluid flow. *Marine and Petroleum Geology*, **66**, 165–
628 176, doi:10.1016/j.marpetgeo.2015.02.003

629 Bigi, S., Conti, A., Casero, P., Ruggiero, L., Recanati, R., Lipparini, L. (2013). Geological model of the central
630 Periadriatic basin (Apennines, Italy). *Marine and Petroleum Geology*, **42**, 107–121. doi:10.1016/j.marpetgeo.2012.07.005.

631 Boccaletti, M., Calamita, F., Deiana, G., Gelati, R., Massari, F., Moratti, G., Ricci Lucchi, F. 1990. Migrating foredeep-
632 thrust belt system in the Northern Apennines and Southern Alps. *Palaeogeography, Palaeoclimatology Palaeoecology*, **77**,
633 3–14.

634 Bradshaw J., Bachu S., Bonijoly D., Burruss R., Holloway S., Christensen N.P. 2007. CO₂ storage capacity estimation:
635 issues and development of standards. *International Journal of Greenhouse Gas Control*, **1**, 62–68.

636 Bradshaw, B. E., Spencer, L. K., Lahtinen, A.-L., Khider, K., Ryan, D. J., Colwell, J. B., Chirinos, A., Bradshaw, J.,
637 Draper, J.J., Hodgkinson, J., McKillop, M. 2011. An assessment of Queensland's CO₂ geological storage prospectivity
638 - The Queensland CO₂ Geological Storage Atlas. *Energy Procedia*, **4**, 4583–4590, doi:10.1016/j.egypro.2011.02.417

639 Brigaud, B., Vincent, B., Durllet, C., Deconinck, J.-F., Jobard, E., Pickard, N., ... Landrein, P. (2014). Characterization
640 and origin of permeability–porosity heterogeneity in shallow-marine carbonates: From core scale to 3D reservoir
641 dimension (Middle Jurassic, Paris Basin, France). *Marine and Petroleum Geology*, **57**, 631–651.
642 doi:10.1016/j.marpetgeo.2014.07.004

643 Buttinelli, M., Procesi, M., Cantucci, B., Quattrocchi, F., Boschi, E. 2011. The geo-database of caprock quality and deep
644 saline aquifers distribution for geological storage of CO₂ in Italy. *Energy*, **36**, 2968–
645 2983. doi:10.1016/j.energy.2011.02.041

646 Calamita, F., Deiana, G. 1988. The arcuate shape of the Umbria-Marche-Sabina Apennines (central Italy).
647 *Tectonophysics*, **146**, 139–147.

648 Cappelletti, F., Casero, P., Colucci F., Costabile, R., Federici, P., Moia, F., Rondena, E., Stella, G., Valagussa, M. 2012.
649 Caratterizzazione di potenziali siti nazionali di stoccaggio geologico della CO₂. Rapporto 12001252, RSE.

650 Carminati, E., Doglioni, C., 2012. Alps vs. Apennines: the paradigm of a tectonically asymmetric Earth. *Earth Science*
651 *Reviews*, **112**, 67–96, <http://dx.doi.org/10.1016/j.earscirev.2012.02.004>

- 652 Carminati, E., Wortel, M. J., Spakman, W., Sabadini, R. 1998. The role of slab detachment processes in the opening of
653 the western–central Mediterranean basins: some geological and geophysical evidence. *Earth and Planetary Science*
654 *Letters*, **160**, 651–665, doi:10.1016/s0012-821x(98)00118-6
- 655 Carrozzo, M.T., Luzio, D., Margiotta, C., Quarta, T., 1990. Gravity map of Italy. In: *Structural Model of Italy and Gravity*
656 *Map*. P.F.G.-CNR, Quaderno 114 de “La Ricerca Scientifica”, 3.
- 657 Casero, P., 2004. Structural Setting of Petroleum Exploration Plays in Italy. In: *Special Volume of the Italian Geological*
658 *Society for the IGC 32 Florence-2004*. 189–199.
- 659 Casero, P., Bigi, S. 2013. Structural setting of the Adriatic basin and the main related petroleum exploration plays. *Marine*
660 *and Petroleum Geology*, **42**, 135–147, doi:10.1016/j.marpetgeo.2012.07.006
- 661 Castellarin, A., 2001. Alps-Apennines and Po Plain frontal Apennines relationships. In: Vai, G.B., Martini, I.P. (eds.),
662 *Anatomy of an Orogen: The Apennines and Adjacent Mediterranean Basins*. Kluwer Academic Publishers, Bodmin, 177–
663 196.
- 664 Cavazza, W., Roure, F.M., Spakman, W., Stampfli, G.M., Ziegler, P.A. (eds.) 2004. *The TRANSMED Atlas, the*
665 *Mediterranean region from crust to mantle*. Springer, Berlin Heidelberg.
- 666 Cazzini, F., Dal Zotto, O., Fantoni, R., Ghielmi, M., Ronchi, P., Scotti, P. 2015. Oil and gas in the Adriatic Foreland,
667 Italy. *Journal of Petroleum Geology*, **38**, 255–279.
- 668 Civile, D., Zecchin, M., Forlin, E., Donda, F., Volpi, V., Merson, B., Persoglia, S. 2013. CO₂ geological storage in the
669 Italian carbonate successions. *International Journal of Greenhouse Gas Control*, **19**, 101–
670 116, doi:10.1016/j.ijggc.2013.08.010
- 671 Colacicchi, R., & Baldanza, A. (1986). Carbonate turbidites in a Mesozoic pelagic basin: Scaglia Formation, Apennines—
672 comparison with siliciclastic depositional models. *Sedimentary Geology*, 48(1-2), 81-105.
- 673 Crain E. R., 1986. *The Log Analysis Handbook*. Pennwell Books.
- 674 Deng, H., Fitts, J. P., Crandall, D., McIntyre, D., & Peters, C. A. (2015). Alterations of fractures in carbonate rocks by
675 CO₂-acidified brines. *Environmental science & technology*, 49(16), 10226-10234.
- 676 DOE-NETL (U.S. Department of Energy – National Energy Technology Laboratory – Office of Fossil Energy), 2006.
677 *Carbon Sequestration Atlas of the United States and Canada*. [http://www.netl.doe.gov/technologies/carbon](http://www.netl.doe.gov/technologies/carbon_seq/refshelf/atlas/)
678 [seq/refshelf/atlas/](http://www.netl.doe.gov/technologies/carbon_seq/refshelf/atlas/).
- 679 DOE-NETL (U.S. Department of Energy – National Energy Technology Laboratory – Office of Fossil Energy), 2008.
680 *Carbon Sequestration Atlas of the United States and Canada*, 2nd ed. [http://www.netl.doe.gov/technologies/carbon](http://www.netl.doe.gov/technologies/carbon_seq/refshelf/atlas/)
681 [seq/refshelf/atlas/](http://www.netl.doe.gov/technologies/carbon_seq/refshelf/atlas/).
- 682 Doglioni, C., Harabaglia, P., Merlini, S., Mongelli, F., Peccerillo, A., Piromallo, C., 1999. Orogens and slabs vs. their
683 direction of subduction. *Earth Science Reviews*, **45**, 167–208.
- 684 Donda, F., Volpi, V., Persoglia, S., Parushev, D., 2011. CO₂ storage potential of deep saline aquifers: the case of Italy.
685 *International Journal of Greenhouse Gas Control*, **5**, 327–335.
- 686 Doughty, C., Pruess, K., Benson, S. M., Hovorka, S. D., Knox, P. R., Green, C. T. 2001. Capacity investigation of brine-
687 bearing sands of the Frio Formation for geologic sequestration of CO₂. *GCCC Texts and Reports*.
- 688 Fabbi, S., Citton, P., Romano, M., & Cipriani, A. (2016). Detrital events within pelagic deposits of the Umbria-Marche
689 Basin (Northern Apennines, Italy): further evidence of Early Cretaceous tectonics. *Journal of Mediterranean Earth*
690 *Sciences*, 8, 39-52
- 691 Freeman, B., Yielding, G., Needham, D. T., & Badley, M. E. 1998. Fault seal prediction: the gouge ratio
692 method. *Geological Society, London, Special Publications*, 127(1), 19-25.
- 693 Ghielmi, M., Minervini, M., Nini, C., Rogledi, S., & Rossi, M. (2013). Late Miocene–Middle Pleistocene sequences in
694 the Po Plain–Northern Adriatic Sea (Italy): the stratigraphic record of modification phases affecting a complex foreland
695 basin. *Marine and Petroleum Geology*, 42, 50-81.
- 696 Geothopica 2010. *Geothermal Resources National Inventory (Italy)*.
- 697 Goodman, A., Hakala, A., Bromhal, G., Deel, D. Rodosta, T., Frailey, S., Small, M., Allen, D., Romanov, V., Fazio, J.,
698 Huerta, N., McIntyre, D., Kutchko, B., Guthrie, G. 2011. US DOE methodology for the development of geologic storage
699 potential for carbon dioxide at the national and regional scale. *International Journal of Greenhouse Gas Control*, **5**,
700 952–965.

- 701 Gorecki, C. D., Sorensen, J. A., Bremer, J. M., Knudsen, D., Smith, S. A., Steadman, E. N., and Harju, J. A. 2009.
702 Development of storage coefficients for determining the effective CO₂ storage resource in deep saline formations. In SPE
703 International Conference on CO₂ Capture, Storage, and Utilization. Society of Petroleum Engineers.
- 704 Gough, C., Shackley, S. 2006. Towards a multi-criteria methodology for assessment of geological carbon storage options.
705 *Climatic Change*, **74**, 141–174.
- 706 Guerreiro, L., Silva, A. C., Alcobia, V., & Soares, A. 2000. Integrated reservoir characterisation of a fractured carbonate
707 reservoir. In SPE International Petroleum Conference and Exhibition in Mexico. Society of Petroleum Engineers.
- 708 Harris, D., Yielding, G., Levine, P., Maxwell, G., Rose, P. T., & Nell, P. (2002). Using Shale Gouge Ratio (SGR) to
709 model faults as transmissibility barriers in reservoirs: an example from the Strathspey Field, North Sea. *Petroleum*
710 *Geoscience*, **8**(2), 167-176.
- 711 Holloway, S., 2005. Underground sequestration of carbon dioxide a viable green-house gas mitigation option. *Energy*,
712 **30**, 2318–2333.
- 713 IEA GHG (International Energy Agency Greenhouse Gas R&D Programme) 2009. Development of Storage Coefficients
714 for CO₂ Storage in Deep Saline Formations. Report No. 2009/13., <http://www.ieaghg.org/>
- 715 IEA-International Energy Agency, 2004. Prospects for CO₂ Capture and Storage. IEA/OECD, Paris, France, p. 249.
- 716 IPCC, 2005. IPCC Special Report on Carbon Dioxide Capture and Storage. Prepared by Working Group III of the
717 Intergovernmental Panel on Climate Change [Metz, B., O. Davidson, H. C. de Coninck, M. Loos, and L. A. Meyer (eds.)].
718 Cambridge University Press, Cambridge, United Kingdom and New York, NY, USA.
- 719 Journel A. G., Alabert F. G. 1989. Non-Gaussian data expansion in the Earth Sciences. *Terra Nova*, **1**, 123–134.
- 720 Kavousi, P., & Gao, D. (2013). Seismic attribute-assisted reservoir property modeling using sequential Gaussian
721 simulation: A case study from the Persian Gulf. In SEG Technical Program Expanded Abstracts 2013 (pp. 2362-2366).
722 Society of Exploration Geophysicists.
- 723 Ketzer, J. M., Machado, C. X., Rockett, G. C., Iglesias, R. S. 2015. Brazilian Atlas of CO₂ capture and geological storage.
724 CEPAC/EDIPUCRS.
- 725 Knopf, S., and May, F. 2017. Comparing methods for the estimation of CO₂ storage capacity in saline aquifers in
726 Germany: regional aquifer based vs. structural trap-based assessments. *Energy Procedia*, **114**, 4710-4721.
- 727 Koopman, A. 1983. Detachment tectonics in the central Apennines, Italy. PhD thesis, Instituut voor Aardwetenschappen
728 RUU.
- 729 Kopp, A., Class, H., Helmig, R. 2009. Investigations on CO₂ storage capacity in saline aquifers: Part 1. Dimensional
730 analysis of flow processes and reservoir characteristics. *International Journal of Greenhouse Gas Control*, **3**, 263–276.
- 731 Kovscek A. R. 2002. Screening criteria for CO₂ storage in oil reservoirs. *Petroleum Science and Technology*, **20**,
732 841–866, DOI: 10.1081/ LFT-120003717
- 733 Luquot, L., and Gouze, P. 2009. Experimental determination of porosity and permeability changes induced by injection
734 of CO₂ into carbonate rocks. *Chemical Geology*, **265**(1-2), 148-159.
- 735 Malinverno, A., Ryan, W.B.F. 1986. Extension in the Tyrrhenian sea and shortening in the Apennines as result of arc
736 migration driven by sinking of the lithosphere. *Tectonics*, **5**, 227–245.
- 737 Marek, S., Dzięwińska, L., and Tarkowski, R. 2011. The possibilities of underground CO₂ storage in the Zaosie
738 Anticline. *Gospodarka Surowcami Mineralnymi*, **27**, 89-107.
- 739 Moia, F., Fais, S., Pisanu, F., Sardu, G., Casero, P., Cappelletti, F., and Colucci, F. 2012. la fattibilità dello stoccaggio
740 geologico della co₂ negli acquiferi salini profondi nell'onshore e offshore italiano. in 1° congresso dei geologi di
741 basilicata-ricerca, sviluppo ed utilizzo delle fonti fossili, il ruolo del geologo (pp. 339-351). dibuono edizioni.
- 742 Nashaat, M. 1998. Abnormally high formation pressure and seal impacts on hydrocarbon accumulations in the Nile Delta
743 and North Sinai basins, Egypt. In: Law, B. E., Ulmishek, G. F., Slavina, V. I. (eds.) *Abnormal pressures in hydrocarbon*
744 *environments*. AAPG Memoir, **70**, 161–180.
- 745 Nezhad, H. K., & Tabatabaei, H. 2017. Simulation of petrophysical parameters of Asmari reservoir using SGS method in
746 Mansuri oil field, Southwest of Iran. *Open Journal of Geology*, **7**(08), 1188.
- 747 Ori, G. G., Roveri, M., Vannoni, F. 1986. Plio-Pleistocene sedimentation in the Apenninic-Adriatic foredeep (Central
748 Adriatic Sea, Italy). In: Allen, P., A., Homewood P. (eds.) *Foreland basins*, **8**, International Association of
749 Sedimentologists, Gent, 183–198.

- 750 Patacca, E., Scandone, P. 2001. Late thrust propagation and sedimentary response in the thrust belt-foredeep system of
751 the southern Apennines (Pliocene-Pleistocene). In: Vai, G.B., Martini, I.P. (eds.) *Anatomy of an Orogen: The Apennines
752 and Adjacent Mediterranean Basins*. Kluwer Academic Publishers, Bodmin, 401–440.
- 753 Patacca, E., Scandone, P. 2004. The Plio-Pleistocene thrust belt-foredeep system in the Southern Apennines and Sicily
754 (Italy). In: Crescenti, V., D'Offizi, S., Merlino, S., Sacchi, L. (eds.) *Geology of Italy*. Società Geologica Italiana. Special
755 Volume IGC 32 Florence, 79–92.
- 756 Peng, C., Anabaraonye, B. U., Crawshaw, J. P., Maitland, G. C., and Trusler, J. M. 2016. Kinetics of carbonate mineral
757 dissolution in CO₂-acidified brines at storage reservoir conditions. *Faraday discussions*, 192, 545-560.
- 758 Petracchini, L., Antonellini, M., Billi, A., Scrocca, D. 2012. Fault development through fractured pelagic carbonates of
759 the Cingoli anticline, Italy: Possible analog for subsurface fluid-conductive fractures. *Journal of Structural Geology*, **45**,
760 21–37, doi:10.1016/j.jsg.2012.05.007
- 761 Ramírez A., Hagedoorn S., Kramers L., Wildenborg T., Hendriks C. 2010. Screening CO₂ storage options in the
762 Netherlands. *International Journal of Greenhouse Gas Control*, **4**, 367–380.
- 763 Raymer, L. L., Hunt, E. R., Gardner, J. S. 1980. An improved sonic transit time-to-porosity transform. 21st Annual
764 Logging Symposium of Society of Petrophysicists and Well-Log Analysts, 8-11 July 1980, Lafayette, Louisiana.
- 765 Riis, F., and Halland, E. 2014. CO₂ Storage Atlas of the Norwegian Continental Shelf: Methods Used to Evaluate
766 Capacity and Maturity of the CO₂ Storage Potential. *Energy Procedia*, **63**, 5258-5265.
- 767 Rosenbaum, G., Lister, G.S., 2004. Formation of arcuate orogenic belts in the western Mediterranean region. In: Sussman,
768 A., Weil, A. (eds.) *Orogenic Curvature*. Special Paper Geological Society of America, **383**, 41–56.
- 769 Ryan, W.B.F., S.M. Carbotte, J.O. Coplan, S. O'Hara, A. Melkonian, R. Arko, R.A. Weissel, V. Ferrini, A. Goodwillie,
770 F. Nitsche, J. Bonczkowski, and R. Zemsky (2009), Global Multi-Resolution Topography synthesis, *Geochem. Geophys.*
771 *Geosyst.*, **10**, Q03014, doi:10.1029/2008GC002332.
- 772 Saftić, B., Kolenković Močilac, I., Cvetković, M., Vulin, D., Velić, J., Tomljenović, B. 2019. Potential for the Geological
773 Storage of CO₂ in the Croatian Part of the Adriatic Offshore. *Minerals*, **9**, 577.
- 774 Smith, D. J., Noy, D. J., Holloway, S., Chadwick, R. A. 2011. The impact of boundary conditions on CO₂ storage capacity
775 estimation in aquifers. *Energy Procedia*, **4**, 4828–4834, doi:10.1016/j.egypro.2011.02.449
- 776 Span R., Wagner W. 1996. A new equation of state for carbon dioxide covering the fluid region from the triple-point
777 temperature to 1100K at pressures up to 800 MPa. *Journal of Physical and Chemical Reference Data*, **25**, 1509-1596.
- 778 Suekane, T., Soukawa, S., Iwatani, S., Tsushima, S., Hirai, S. 2005. Behavior of supercritical CO₂ injected into porous
779 media containing water. *Energy*, **30**, 2370–2382.
- 780 Tavani, S., Storti, F., Salvini, F., Toscano, C. 2008. Stratigraphic versus structural control on the deformation pattern
781 associated with the evolution of the Mt. Catria anticline, Italy. *Journal of Structural Geology*, **30**, 664–681.
- 782 Teatini, P., Castelletto, N., Gambolati, G. 2014. 3D geomechanical modeling for CO₂ geological storage in faulted
783 formations. A case study in an offshore northern Adriatic reservoir, Italy. *International Journal of Greenhouse Gas
784 Control*, **22**, 63–76, doi:10.1016/j.ijggc.2013.12.021
- 785 Terzaghi von K. 1925. *Erdbaumechanik auf bodenphysikalischer Grundlage*. Leipzig u. Wien, Franz Deuticke.
- 786 Terzaghi von K. 1936. The shearing resistance of saturated soils and the angle between the planes of shear. In: Casgrande,
787 A.; Rutledge, P. C.; Watson; J. D. (eds.) *Proceedings of International Conference of Soil Mechanics and Foundation
788 Engineering*, Vol. I, 54–56. Harvard University.
- 789 Trippetta, F., Durante, D., Lipparini, L., Romi, A., & Brandano, M. 2021. Carbonate-ramp reservoirs modelling best
790 solutions: Insights from a dense shallow well database in Central Italy. *Marine and Petroleum Geology*, **126**, 104931.
- 791 Van der Meer, L. B., Yavuz, F. 2009. CO₂ storage capacity calculations for the Dutch subsurface. *Energy Procedia*, **1**,
792 2615–2622.
- 793 Vangkilde-Pedersen, T., Anthonsen, K. L., Smith, N., Kirk, K., van der Meer, B., Le Gallo, Y., Bossie-Codreanu, D.
794 Wojcicki, A., Le Nindre, Y.M., Hendriks C., Dalhoff, F., Christensen, N.P. 2009a. Assessing European capacity for
795 geological storage of carbon dioxide—the EU GeoCapacity project. *Energy Procedia*, **1**, 2663–2670.
- 796 Vangkilde-Pedersen, T., Kirk, K., Smith, N., Maurand, N., Wojcicki, A., Neele, F., ... & Lyng Anthonsen, K. 2009b. EU
797 GeoCapacity—Assessing European Capacity for Geological Storage of Carbon Dioxide. D42 GeoCapacity Final Report;.
- 798 Venisti, N., Calcagnile, G., Gaudio, V. D., Pierri, P. 2004. Combined analysis of seismic and gravimetric data in the
799 Adriatic plate. *Physics of the Earth and Planetary Interiors*, **142**, 89–100, doi:10.1016/j.pepi.2003.12.012

800 Verly, G. 1993. Sequential Gaussian Simulation: A Monte Carlo Method for Generating Models of Porosity and
801 Permeability. *Generation, Accumulation and Production of Europe's Hydrocarbons III*, 345–356, doi:10.1007/978-3-642

802 Volpi, V., Forlin, F., Donda, F., Civile, D., Facchin, L., Sauli, S., Merson B., Sinza-Mendieta, K., Shams, A.
803 2014. Southern Adriatic Sea as a Potential Area for CO₂ Geological Storage. *Oil & Gas Science and Technology - Revue*
804 *d'IFP Energies Nouvelles*, **70**, 713–728, doi:10.2516/ogst/2014039

805 Williams, J. D. O., Jin, M., Bentham, M., Pickup, G. E., Hannis, S. D., & Mackay, E. J. (2013). Modelling carbon dioxide
806 storage within closed structures in the UK Bunter Sandstone Formation. *International Journal of Greenhouse Gas*
807 *Control*, *18*, 38-50.

808 Wright, R., Mourits, F., Rodríguez, L. B., Serrano, M. D. 2013. The first North American carbon storage atlas. *Energy*
809 *Procedia*, **37**, 5280–5289.

810 Wyllie, M. R. J., Gardner, G. H. F., Gregory, A. R. 1962. Studies of elastic wave attenuation in porous media. *Geophysics*,
811 **27**, 569–589.

812 Wyllie, M. R. J., Gregory, A. R., Gardner, G. H. F. 1958. An experimental investigation of factors affecting elastic wave
813 velocities in porous media, *Geophysics*, **23**, 459–493.

814 Wyllie, M. R. J., Gregory, A. R., Gardner, L. W. 1956. Elastic wave velocities in heterogeneous and porous media.
815 *Geophysics*, **21**, 41–70.

816 Xu, Y., Cavalcante Filho, J. S., Yu, W., & Sepehrnoori, K. (2017). Discrete-fracture modeling of complex hydraulic-
817 fracture geometries in reservoir simulators. *SPE Reservoir Evaluation & Engineering*, 20(02), 403-422.
818

819 Yielding, G., Freeman, B., & Needham, D. T. 1997. Quantitative fault seal prediction. *AAPG bulletin*, 81(6), 897-
820 917. Harris, D., Yielding, G., Levine, P., Maxwell, G., Rose, P. T., & Nell, P. 2002. Using Shale Gouge Ratio (SGR) to
821 model faults as transmissibility barriers in reservoirs: an example from the Strathspey Field, North Sea. *Petroleum*
822 *Geoscience*, 8(2), 167-176.

823 Zappaterra, E. 1990. Carbonate paleogeographic sequences of the Periadriatic region. *Bollettino della Società Geologica*
824 *Italiana*, **109**, 5–20.

825 Zare, A., Bagheri, M., & Ebadi, M. 2020. Reservoir facies and porosity modeling using seismic data and well logs by
826 geostatistical simulation in an oil field. *Carbonates and Evaporites*, 35, 1-10.